

Fluid permeability in porous media: Comparison of electrical estimates with hydrodynamical calculations

Sergio Kostek, Lawrence M. Schwartz, and David Linton Johnson

Schlumberger-Doll Research, Old Quarry Road, Ridgefield, Connecticut 06877-4108

(Received 2 July 1991)

The principal dimensionless quantities used to characterize the geometry of porous media are the porosity ϕ and the electrical formation factor F . However, many properties of interest (e.g., nuclear magnetic relaxation, mercury porosimetry, and viscous fluid flow) depend on the absolute dimensions of the pore space. Among the most important pore scale lengths are the pore volume to surface area ratio V_p/S , the Λ parameter, and the diffusion-limited surface trapping length w_s . We have calculated these lengths for two- and three-dimensional geometrical models of porous media and have used each of them to estimate the permeability k to viscous fluid flow as determined by direct numerical solution of the Stokes equations. Our analysis is based on three families of geometrical models: (1) three-dimensional ordered sphere packs (including the consolidation regime), (2) two-dimensional tortuous-path models, and (3) two-dimensional Koch-curve models. In all cases we find that the rigorous bound recently formulated in terms of w_s provides rather a weak constraint when compared to the actual value of k . In the sphere-pack models, permeability estimates based on V_p/S are reasonably accurate, but such estimates are much less valuable in the more interesting two-dimensional geometries. Our most important finding is that in *all* the cases examined the Λ -parameter estimate of permeability is quite reliable. Nevertheless, in the Koch-curve models, as the effective channel cross-sectional area narrows, we are able to see evidence for the breakdown of this estimate. This breakdown is associated with differences in the singularities of the Stokes and Laplace solutions in the vicinity of jagged constrictions in the flow paths.

I. INTRODUCTION

Given a sample of porous material of length L across which there is an applied pressure difference ΔP , the macroscopic flow of a viscous fluid is described by Darcy's law^{1,2}

$$V = -\frac{k}{\eta} \frac{\Delta P}{L}, \quad (1)$$

where η is the fluid's viscosity and k is the permeability. Equation (1) is analogous to Ohm's law for the flow of electrical current, and k is the counterpart of the effective conductivity. We emphasize, however, that k depends on both the tortuosity of the pore space and on the absolute dimensions of the pores. (By contrast the electrical formation factor F [see Eq. (3) below] is scale invariant.) Indeed, k has the dimensions of area and may be thought of as representing the cross section of an effective channel for fluid flow through the pore space. There is in the literature a number of empirical techniques for estimating k .³⁻⁸ Each of these is based on the inference of an appropriate pore-size parameter from an independent measurement. While such empirical methods can be of practical value, they represent uncontrolled approximations and usually provide little insight as to the physical basis for the observed correlation.

In the present paper our aim is to examine several model pore geometries, and in each case to assemble a number of relevant pore scale parameters. By so doing, we hope to test the fundamental basis for alternate permeability estimation techniques and, more generally, to illuminate the properties of different pore length scales.

In particular, we will focus on three characteristic length scales. First is the pore volume to surface area ratio V_p/S . Second is the Λ parameter, a length that arises naturally in the description of interfacial electrical conduction⁹ and third, is the diffusion-limited trapping length, w_s . This last length is of particular interest because Torquato¹⁰ has recently shown that w_s can be used to construct a rigorous bound on the permeability.

In addition to these parameters, various authors have proposed schemes for estimating k using an effective pore size derived from mercury injection experiments.^{3,4} Within a simplified theoretical framework, the existence of a correlation between these two fluid flow measurements can be justified based on percolation theory arguments.^{4,11} It can, in fact, be shown (under the same assumptions) that the pore sizes obtained from the mercury capillary pressure curve and the Λ parameter are directly proportional.¹¹

In Sec. II we summarize the basic equations used to calculate the various pore scale lengths under consideration. We discuss also the direct calculation of the permeability. In Sec. III the exact values of k are compared with different estimates formulated in terms of V_p/S , Λ , and w_s for three model geometries with widely varying physical properties. Our conclusion, based on this analysis, is that Λ provides by far the most reliable estimates of k . In a sense, this is not surprising because Λ is, itself, directly based upon a transport problem, although of a very different nature. Finally, we discuss the nature of the singularities encountered in the solution of the Stokes and Laplace equations¹² and their implications for the validity of permeability estimates based on the Λ parameter.

II. THEORETICAL BACKGROUND

A. Electrical conductivity: The Λ parameter

Suppose we have an insulating porous medium saturated with a single fluid whose conductivity takes the uniform value σ_f . If an electrostatic potential difference, ΔU , is applied across the system, the local electrostatic potential, $U(\mathbf{r})$, satisfies Laplace's equation

$$\nabla^2 U(\mathbf{r}) = 0, \quad (2)$$

with the boundary condition $\mathbf{E}(\mathbf{r}) \cdot \hat{\mathbf{n}} \equiv -\nabla U(\mathbf{r}) \cdot \hat{\mathbf{n}} = 0$, where $\hat{\mathbf{n}}$ is a unit normal vector directed into the grain space. The total current \mathbf{J} is then obtained by integrating the local contributions $\mathbf{j}(\mathbf{r}) \equiv \sigma_f \mathbf{E}(\mathbf{r})$ and the effective conductivity of the porous medium is $J = \sigma_{\text{eff}} \Delta U$. A useful dimensionless parameter characterizing the effective resistance to current flow is the formation factor

$$F \equiv \frac{\sigma_f}{\sigma_{\text{eff}}}. \quad (3)$$

F , unlike k , is a *scale invariant* quantity; if we uniformly magnify or shrink the sizes of the pores and grains, leaving the porosity unchanged, the value of F is unaffected. Nevertheless, the electrical conduction problem does provide a framework for the introduction of useful pore-size parameters. In the study of interfacial conduction a quantity that arises naturally is the Λ parameter:⁹

$$\frac{\Lambda}{2} \equiv \frac{\int |\mathbf{E}(\mathbf{r})|^2 dV_p}{\int |\mathbf{E}(\mathbf{r})|^2 dS} \neq \frac{V_p}{S}. \quad (4)$$

Here V_p is the pore volume and S is the surface area of the pore-grain interface. The quantity V_p/S is a simple *geometrical* length that can, in principle, be measured by stereological techniques.¹³ By contrast, Λ is a *dynamical* length determined by the solutions of Laplace's equation and cannot be measured by geometrical analysis. Note that Λ is a length that is directly related to transport; regions of the pore space in which the electric field vanishes do not contribute to Λ ; this length is, in some sense, a measure of the *dynamically connected* part of the pore space. (Note that in the special case in which the pores are cylindrical tubes of radius R , the electric field is uniform, and $\Lambda = R$).

B. The diffusion-limited trapping length

Consider a problem in which particles are initially distributed with uniform density in the pore space and are then allowed to diffuse randomly but are removed as soon as they reach the pore-grain interface. In the Laplace transform domain, the relevant equations are^{10,14}

$$D \nabla^2 u(\mathbf{r}) = -1 \quad \text{in } V_p; \quad u(\mathbf{r}) = 0 \quad \text{on } S, \quad (5)$$

where D is the diffusion constant of the pore fluid. It can then be shown that the average lifetime for particles subject to this decay process is given by¹⁴

$$\tau_s = \frac{1}{V_p} \int u(\mathbf{r}) dV_p = \frac{D}{V_p} \int |\nabla u(\mathbf{r})|^2 dV_p \equiv \frac{w_s^2}{D}. \quad (6)$$

w_s has the dimensions of a length and is the characteristic measure of pore size relevant to diffusion-limited interface trapping; its value is independent of D . Like the Λ parameter, w_s is a length defined by a physical problem and does not have a purely geometrical interpretation. In the present context, w_s is of interest because Torquato¹⁰ has recently derived an inequality relating the fluid permeability k , the porosity, ϕ , and the mean lifetime for the surface diffusion problem:

$$k \leq k_D \equiv \phi D \tau_s = \phi w_s^2. \quad (7)$$

For anisotropic media this inequality holds for each principal component of the permeability tensor.

C. Hydrodynamical calculations

In the limit of slow incompressible flow, the Navier-Stokes equations reduce to the linear Stokes equations^{1,2}

$$\eta \nabla^2 \mathbf{v}(\mathbf{r}) = \nabla p(\mathbf{r}), \quad \nabla \cdot \mathbf{v}(\mathbf{r}) = 0, \quad (8)$$

where \mathbf{v} and p are, respectively, the local velocity and pressure fields, and η is the fluid viscosity. The fluid velocity must vanish at the pore-grain interface and a prescribed pressure difference at the inlet and outlet faces is assumed. In three dimensions, accurate solutions of the Stokes equations are available only in the case of ordered systems in which the geometry of the pores and grains is relatively simple. For example, Larson and Higdon¹⁵ have recently evaluated the permeability for simple cubic (sc), face-centered cubic (fcc), and body-centered cubic (bcc) packings of spherical grains. They consider the complete range of porosities, from the dilute sphere limit to overlapping (i.e., consolidated) spheres at the other extreme. To take advantage of the grain shape, Larson and Higdon¹⁵ expand the velocity and pressure fields in terms of spherical harmonics. The expansion coefficients are determined by imposing the nonslip boundary condition at the remaining surfaces of the unit cell. This approach is efficient and accurate, but is only feasible because the models considered in Ref. 15 exhibit so high a degree of symmetry. For the two-dimensional models of interest in the present paper these techniques are not practical. Instead, we solve Eqs. (8) by the finite-element method.¹⁶

III. RESULTS FOR MODEL SYSTEMS

In many nontrivial porous systems, the pore space consists of large open regions (pores) connected by narrow throats. While the pores account for most of the porosity, it is the throats that limit the transport. To understand how well the different pore lengths scales introduced above are interrelated, and to what extent they can be used to estimate permeability, we will consider three families of geometrical models. In each case exact numerical calculations of k will be compared with three permeability estimates. First is the Kozeny-Carman relation¹

$$k_{\text{KC}} = \begin{cases} \frac{(2V_p/S)^2}{12F} & \text{(two dimensions),} \\ \frac{(2V_p/S)^2}{8F} & \text{(three dimensions).} \end{cases} \quad (9)$$

In these equations $2V_p/S$ is the effective channel diameter and F takes account, approximately, of the pore space tortuosity. [Equations (9) would yield the correct answer if the two-dimensional pore space were comprised of winding capillary tubes with *uniform radii*.] In the second estimate $2V_p/S$ is replaced by the dynamic length Λ [recall Eq. (4)]

$$k_{\Lambda} = \begin{cases} \frac{\Lambda^2}{12F} & \text{(two dimensions),} \\ \frac{\Lambda^2}{8F} & \text{(three dimensions).} \end{cases} \quad (10)$$

(The motivation for these relations is discussed in Refs. 7, 9, and 11). Third, we consider the estimate provided by the bound of Eq. (7)

$$k_D = \phi w_s^2. \quad (11)$$

A. Three-dimensional grain consolidation (GC) model

Here we begin with an ordered packing of solid spheres and vary the porosity of the system by allowing the spheres to expand uniformly.¹⁷ For an sc packing the spheres touch at $\phi = 1 - \pi/6 \approx 0.476$. Below this porosity the grains are consolidated but the pore space remains interconnected until a threshold is reached at $\phi_c \approx 0.0349$.¹⁷ We have solved Laplace's equation for this model by imposing a uniform cubic grid (with 240 grid points per cube edge in the unit cell) on the system and solving the resulting network equations by the conjugate gradient technique. The results are shown in Fig. 1 together with the calculations of Sheng and Zhou.¹⁸ The formation factors calculated in Ref. 18 are generally higher than our results and the differences grow as $\phi \rightarrow \phi_c$. It is of interest to compare these numerical calculations with an approximation based on "lubrication theory."¹⁵ Here, one pretends that the conducting path has a slowly varying cross-sectional area and that the resistance is simply the series integral of the individual contributions:

$$F = a \int_{-a/2}^{a/2} \frac{dz}{A(z)}, \quad (12)$$

where the z axis is the direction of current flow, a is the cube edge, and $A(z)$ is the pore space area in each plane of constant z . The dotted curve in Fig. 1 represents a direct numerical integration of Eq. (12) and is seen to be in good agreement with our finite-difference results. This is encouraging because lubrication theory becomes increasingly accurate as $\phi \rightarrow \phi_c$, and the electrical resistance is increasingly dominated by the narrow throats.

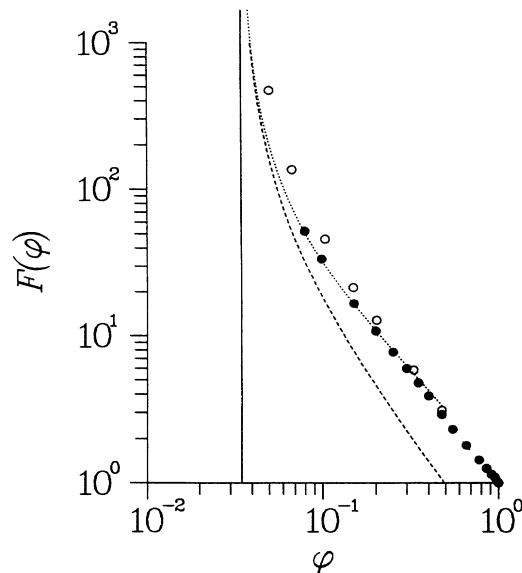


FIG. 1. Electrical formation factor of the simple cubic GC model is shown as a function of porosity ϕ . Shown are: finite-difference calculations (filled circles), finite-element calculations of Ref. 18 (open circles), lubrication theory (dotted line), and asymptotic formula (15) (dashed line). The vertical line indicates the position of the percolation threshold.

Let us consider, then, the behavior of the transport properties near the connectivity threshold ϕ_c . We can derive an analytic expression from Eq. (12) by recognizing that the channel cross-sectional area tends, in this limit, to a square (rotated 45° around the z axis) whose cube edge varies quadratically with z :

$$\lim_{\phi \rightarrow \phi_c} A(z) = [2l_0 + z^2/R]^2. \quad (13)$$

Here $R = a/\sqrt{2}$ is the radius of the sphere in the limit and $2l_0$ is the minimum opening of the throat. We may relate l_0 to the porosity by observing that if the sphere radius is increased by an amount l_0 , the porosity will decrease exactly to ϕ_c :

$$\phi - \phi_c = l_0 S_c / a, \quad (14)$$

where S_c/a is the ratio of surface area to sample volume at ϕ_c . It is a matter of geometry to show that $S_c = \pi(3\sqrt{2} - 4) \approx 0.76$. Finally, the limits of integration in Eq. (12) may safely be extended to $\pm \infty$. The result is

$$\lim_{\phi \rightarrow \phi_c} F(\phi) = \frac{\pi}{8} 2^{1/4} S_c^{3/2} (\phi - \phi_c)^{-3/2}. \quad (15)$$

The exponent of $\frac{3}{2}$ in this equation has been noted earlier;¹⁹ for the well-defined geometry of the GC model we can evaluate the prefactor exactly. Equation (15) is also plotted in Fig. 1.

Consider next, the variation of Λ with porosity. Once Laplace's equation has been solved at each porosity, Λ can be evaluated either from the definition (4) or the relation⁹

$$\frac{2}{\Lambda} = -\frac{d[\ln F]}{d[\ln \phi]} \frac{S}{V_p} \equiv m(\phi) \frac{S}{V_p}. \quad (16)$$

[Equation (16) can be used only when the porosity is changed by uniform growth of the solid phase into the pore space, as in the GC model.] To implement (16), we fit a polynomial, $g(z) = \sum_{n=0}^N a_n z^n$, through the $\ln F$ vs $\ln \phi$ data shown in Fig. 1 [viz. $\ln F \approx g(\ln \phi)$]. A simple derivative of the smooth fit, together with a direct analytic evaluation of V_p/S , then gives Λ . Calculations based on the application of these two methods to our numerical data are summarized in Fig. 2. Regarding our finite-difference calculations, we have found, in practice, that the values of Λ calculated directly from the definition, Eq. (4), converge slowly as the mesh size is decreased. By contrast the formation factor $F(\phi)$ is very well converged, even for fairly coarse grids. For this reason we believe that calculations of Λ based on Eq. (16) (the solid curve of Fig. 2) are the more reliable; as the mesh size is decreased, the black circles in Fig. 2 slowly converge toward the solid line. We note that a direct comparison of our results with the values of Λ calculated in Ref. 18 is not meaningful because Eq. (31) used to define Λ in Ref. 18 is *not* equivalent to our Eq. (4). (See note added in proof.) In the asymptotic limit, the combination of Eqs. (15) and (16) yields

$$\lim_{\phi \rightarrow \phi_c} \Lambda = \frac{4a}{3S_c} (\phi - \phi_c)^{-1}, \quad (17)$$

which is plotted as the dashed line in Fig. 2. The solid curve deviates slightly from the asymptotic result because the fitting curve $g(z)$ used to get $m_s(\phi)$ was not constrained to agree with Eq. (15).

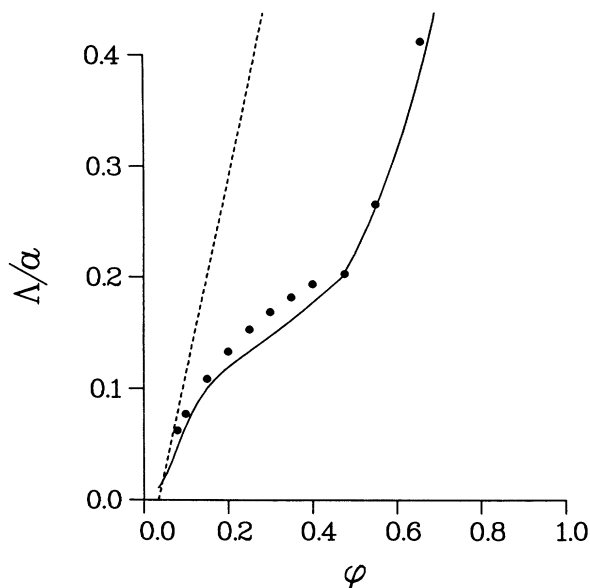


FIG. 2. Two numerical calculations of the Λ parameter are compared with the asymptotic formula (17) (dashed line) for the simple cubic GC model. Shown are an evaluation based on Eq. (4) and finite-difference calculations (filled circles) and an evaluation based on Eq. (16) and finite-difference calculations (solid curve). The unit of length is taken equal to the cube edge in the sc unit cell.

Let us now turn to a discussion of the fluid-flow permeability. In Fig. 3 we plot the numerical results of Larson and Higdon¹⁵ and Sheng and Zhou¹⁸ together with three permeability estimates. The Kozeny-Carman result, Eq. (9) [based on the finite-difference results for $F(\phi)$ shown in Fig. 1], works reasonably well except that it clearly has the wrong asymptotic properties in the limit $\phi \rightarrow \phi_c$. (See below.) Consider next the estimate given by the Λ parameter, Eqs. (10) and (16). Clearly, these equations provide an excellent estimate of permeability over the entire range of porosities in the consolidated regime and, especially, in the vicinity of the connectivity threshold, $\phi \approx \phi_c$. By contrast, in this regime the surface trapping length, w_s , yields rather a poor estimate of k . (w_s is easily calculated for the GC model by random walk simulations.¹⁴) In the high-porosity regime the diffusion bound overestimates the permeability by roughly a factor of $\frac{3}{2}$. However, as $\phi \rightarrow \phi_c$ transport (of any kind) is limited by the closing of the narrow channel cross-sectional areas between the pores while w_s measures an effective pore size which is insensitive to this effect. In the limit $\phi \rightarrow \phi_c$, Larson and Higdon have already shown that lubrication theory is in excellent agreement with their numerically calculated results. We can, however, derive a simple analytic result analogous to Eq. (15). Using, again, the fact that the channel cross-sectional area may be viewed as a square duct of size $2w(z) = (2l_0 + z^2/R)$, the limiting form is

$$\frac{1}{k} = \frac{a}{\beta} \int_{-\infty}^{+\infty} \frac{dz}{[w(z)]^4}, \quad (18)$$

where $\beta = 0.5623$, as defined in Ref. 15. The integral in

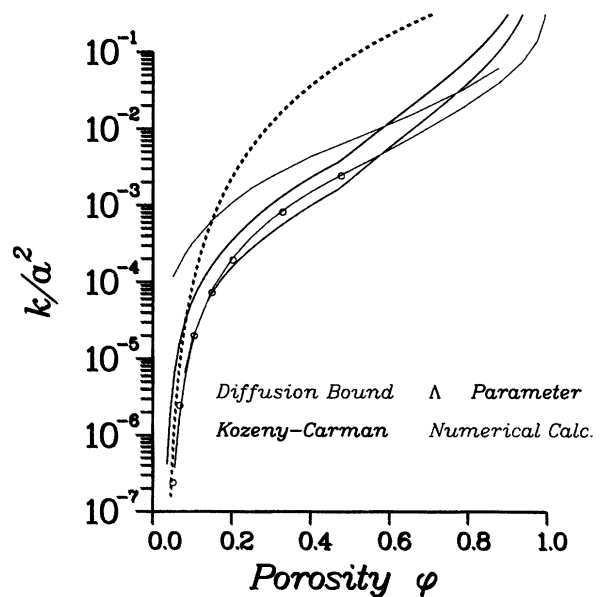


FIG. 3. For the simple cubic GC model, exact calculations of the permeability (solid cyan line, Ref. 15; open cyan circles, Ref. 18) are compared with the Kozeny-Carman and Λ -parameter estimates, with the diffusion bound (Ref. 10), and with the asymptotic formula (19) (dashed line). The values of Λ used here are the ones shown in the solid curve of Fig. 2. Here the length units are as in Fig. 2.

Eq. (18) is readily evaluated with the result

$$\lim_{\phi \rightarrow \phi_c} k(\phi) = \frac{16\beta}{5\pi} 2^{-1/4} \left[\frac{\phi - \phi_c}{S_c} \right]^{7/2} a^2. \quad (19)$$

This formula is plotted as the dashed line in Fig. 3 where it is seen that the numerical results as well as the Λ -parameter estimate appear to converge to it.

Figure 3 involves nearly seven decades of variation in k . A more revealing test of alternate permeability estimates is achieved by examining (Fig. 4) the ratio $M \equiv k/k_{\text{est}}$. Although there is scatter in our M_Λ data, it is clear that values are tending to a constant at the connectivity threshold. This behavior is shown more smoothly by the lubrication theory results. That this is a rigorously correct result can be seen from the asymptotic expressions derived above, Eqs. (15), (17), and (19):

$$\lim_{\phi \rightarrow \phi_c} M_\Lambda(\phi) = M_\Lambda(\phi_c) \equiv \frac{9}{5}\beta \approx 1.012. \quad (20)$$

This limiting value, indicated in Fig. 4 is slightly different from the value appropriate to a straight, square cylinder, which is $M = 2\beta$. We have shown, therefore, that the Λ parameter provides an extremely accurate estimate of the permeability throughout the entire range of porosity from the point where the spheres touch, $\phi \approx 47\%$, down to the connectivity threshold $\phi = \phi_c$. Moreover, the Kozeny-Carman estimate, k_{KC} , and the diffusion bound (7) are seen to give relatively poor estimates of the permeability near the connectivity threshold. [M_{KC} tends to zero at ϕ_c because the exponents in Eqs. (15) and (19) are not equal.]

This result for the behavior of k near the percolation

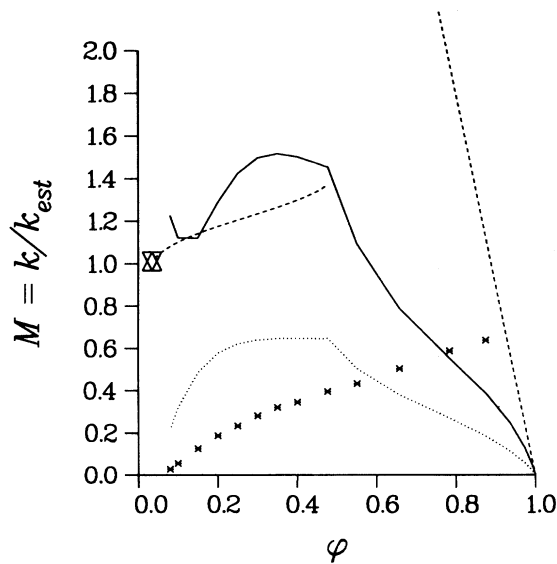


FIG. 4. The Kozeny-Carman, Λ parameter, and diffusion estimates shown in Fig. 3 are replotted here to show the variation of $M \equiv k/k_{\text{est}}$. (Solid line: Λ , dotted curve: Kozeny-Carman, and stars: diffusion bound.) The exact limiting value as $\phi \rightarrow \phi_c$ is indicated by the double triangle. The dashed lines show the results of lubrication theory at low porosities and the asymptotic formula (25) at high porosities.

threshold is not an artifact of the simple cubic lattice, either. First, it is straightforward to repeat the derivation of Eq. (20) for the fcc and bcc lattices. Here, the throats are triangular in shape, as described by Larson and Higdon, who have calculated the relevant values of β . The general expression, valid for all three lattices, is $M_\Lambda(\phi_c) = 36\beta/(5A_c)$, where A_c is defined such that the area of the limiting throat is $A_c l^2$ with l defined in Ref. 15; $A_c = 4, 3\sqrt{3},$ and $4\sqrt{2}$ for sc, fcc, and bcc lattices, respectively. The numerical results are

$$\text{sc: } M_\Lambda(\phi_c) = 1.012, \quad (21a)$$

$$\text{fcc: } M_\Lambda(\phi_c) = 1.080, \quad (21b)$$

$$\text{bcc: } M_\Lambda(\phi_c) = 1.090. \quad (21c)$$

Second, let us consider, briefly, the situation in the disordered GC model appropriate to systems such as fused glass beads. Feng, Halperin, and Sen¹⁹ have argued that the transport properties in these disordered systems near the connectivity threshold are simply related to t , the conductivity exponent for ordinary percolation theory:

$$F \propto (\phi - \phi_c)^{-(t+1/2)}, \quad (22a)$$

$$k \propto (\phi - \phi_c)^{(t+5/2)}. \quad (22b)$$

Because the decrease in porosity can again be viewed as originating from the uniform growth of the insulating phase into the pore space, Eq. (16) is again valid and we have, for the disordered GC model

$$\lim_{\phi \rightarrow \phi_c} M_\Lambda(\phi) = \text{const}, \quad (23)$$

a result that is consistent with experimental data on fused glass beads.⁷ A major conclusion of this paper is that M_Λ is a constant of order unity over the entire range of porosity from the unconsolidated limit down to the connectivity threshold, for ordered as well as disordered GC models. Equation (23) was anticipated in another context by Banavar, Cieplak, and Johnson.²⁰

In what systems might we expect k_Λ to be a poor estimator of permeability? From Fig. 4 we see that in the high-porosity limit of the simple cubic GC model the values of M_Λ tend to zero. In this limit of a dilute concentration of spheres of radius R it is simple to solve for the limiting behavior of all the relevant quantities:

$$\lim_{\phi \rightarrow 1} F = 1 + \frac{3}{2}(1 - \phi), \quad (24a)$$

$$\lim_{\phi \rightarrow 1} k = \frac{2R^2}{9(1 - \phi)}, \quad (24b)$$

$$\lim_{\phi \rightarrow 1} \Lambda = \frac{4R}{9(1 - \phi)}. \quad (24c)$$

Therefore,

$$\lim_{\phi \rightarrow 1} M_\Lambda = 9(1 - \phi). \quad (25)$$

This asymptotic limit is plotted in Fig. 4. The reason why k_Λ provides a poor estimate in this limit is that there are two widely differing relevant sizes, the sphere radius

TABLE I. Summary of results for two-dimensional tortuosity models. k_{FE} denotes the permeability value obtained by the solution of the finite-element equations. The unit of length is one (grain) box length (i.e., $\frac{1}{24}$ of the system's horizontal length).

	ϕ	V_p/S	F	Λ	w_s	k_{FE}
<i>A</i>	0.677	0.826	2.121	1.249	0.524	0.0509
<i>B</i>	0.620	0.659	2.565	1.037	0.410	0.0291
<i>C</i>	0.575	0.594	2.971	0.977	0.361	0.0231
<i>D</i>	0.528	0.554	3.801	0.920	0.339	0.0168

and the cube edge, which enter k , F , and Λ in very different ways. In a similar vein, Saeger, Scriven, and Davis²¹ have shown that whenever transport is limited by flow through an orifice, $M_\Lambda \rightarrow \infty$ because of the differing nature of the singularities in Stokes flow and in potential flow. In the next section we explicitly consider a similar effect involving flow past corners.

B. Two-dimensional tortuous-path model

In the simple cubic GC model the flow paths are essentially one-dimensional sinuous channels. To study the

effects of channels that bend and wind we have examined the sequence of four models shown in Fig. 5. Models of this kind were introduced by Rothman to demonstrate the feasibility of calculating k by lattice gas automaton (LGA) simulations.^{22,23} (Because such simulations are carried out on a triangular lattice, the individual boxes shown in Fig. 5 are rectangular, with a height to width ratio of $\sqrt{3}/2$.) Finite-element techniques¹⁶ have been used to compute the fluid flow patterns shown in Fig. 5 and the value of k for each of the four models. (The relation between the finite element and cellular automata calculation is discussed in Ref. 22.) The electric fields, effective conductivity, and Λ parameter were calculated

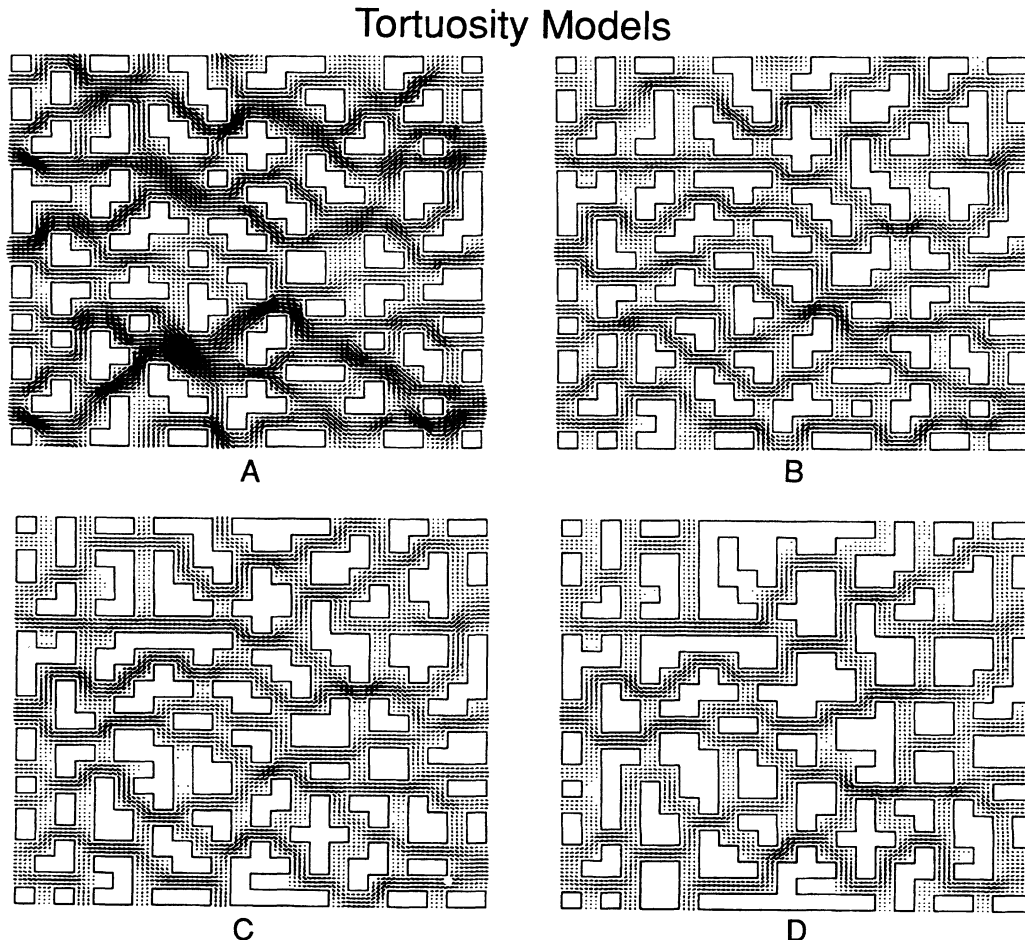


FIG. 5. The four two-dimensional tortuous-path models are pictured with the fluid-flow vectors shown in their pore spaces.

Two-Dimensional Tortuosity Models

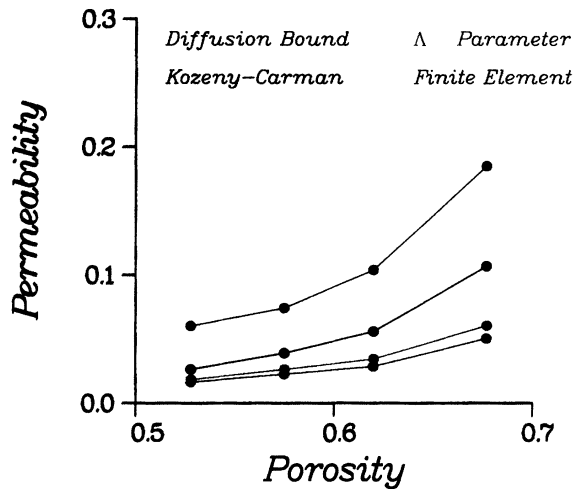


FIG. 6. For the tortuous-path models, exact calculations of the permeability are compared with the Kozeny-Carman and Λ -parameter estimates, and with the diffusion bound of Eq. (7). The unit of length is chosen as in Table I.

by imposing a fine grained equivalent resistor network on each pore space and solving the resulting systems of linear equations by standard conjugate gradient techniques. As expected the flow patterns for the electric current are essentially identical to those of the fluid. Finally, the length w_s was calculated by a random-walk simulation similar to that employed for the GC models.

The results of our calculations are summarized in Table I and Fig. 6. Here we see that k changes by roughly a factor of 3 in response to a change of only about 25% in ϕ . Clearly the Λ parameter provides an excellent approximation to the exact permeability. Interestingly, the Kozeny-Carman and diffusion estimates improve as the porosity is decreased (exactly opposite to the situation encountered in the GC model). Here, at low porosities, the pore channels become more nearly one dimensional and their width is essentially constant. In the high-porosity regime the contrast between pore and throat sizes is much greater, and the physics of fluid transport is well described only by the Λ estimate. Interestingly, the ratio $M_D \equiv k/k_D$ equals roughly $\frac{1}{3}$ and does not vary appreciably with porosity. As the pore geometry evolves, it appears that the diffusion length w_s is relatively insensitive to the changing character of the flow channels.

Koch-Curve Models

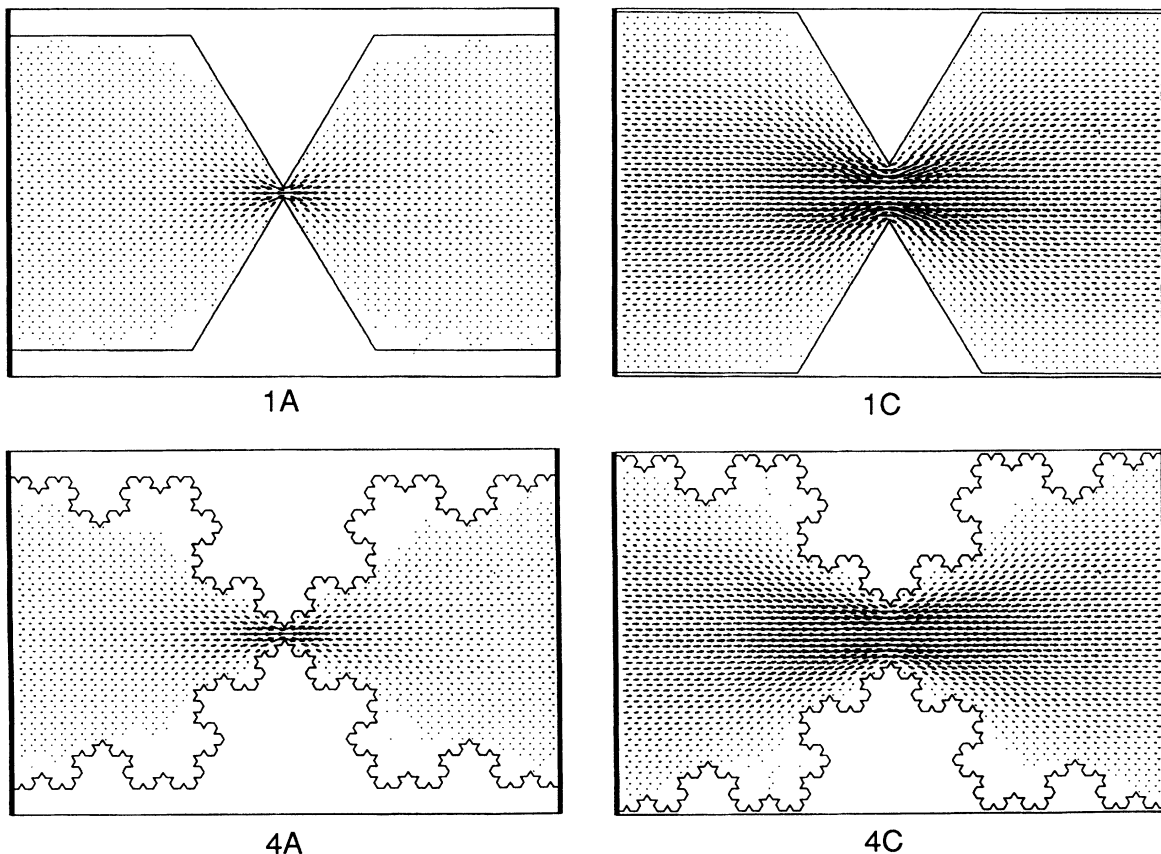


FIG. 7. The four extreme cases of the two-dimensional Koch-curve models are shown. In the upper panel we have the models with the smallest (left) and largest (right) channel cross-sectional sizes, both for the case of smooth pore-grain interfaces. The corresponding situation for the maximum interface roughness is shown in the lower panel. As in Fig. 5, the fluid-flow field is represented within each pore space.

TABLE II. Summary of results for two-dimensional fractal models. k_{FE} denotes the permeability value obtained by the solution of the finite-element equations. The unit of length is the horizontal row separation, $h \equiv 2\epsilon/3^{1/2}$, where ϵ is the grid spacing. The three channel cross-sectional sizes δ are $\delta=6h$ (models 1A, 3A, and 4A), $\delta=18h$ (models 1B, 3B, and 4B), and $\delta=30h$ (models 1C, 3C, and 4C).

Koch-curve model	ϕ	V_p/S	F	Λ	w_s	k_{FE}
1A	0.7194	52.886	2.794	25.03	37.41	6.488
1B	0.7806	57.352	2.153	45.96	39.46	47.80
1C	0.8418	61.858	1.829	64.83	41.53	129.41
3A	0.5426	22.437	3.52	25.47	30.33	6.18
3B	0.6038	24.959	2.65	44.55	32.36	41.51
3C	0.6650	27.495	2.20	63.03	34.65	110.07
4A	0.5184	12.852	3.71	26.18	30.36	5.77
4B	0.5796	17.975	2.74	49.17	32.51	39.34
4C	0.6408	19.874	2.25	61.71	34.72	106.11

C. Two-dimensional Koch-curve model

In dealing with real porous media, one is often interested in the rough or fractal character of the pore-grain interface.^{24–26} In this connection, a two-dimensional model based on the Koch-curve construction is useful in studying the influence of interface roughness on transport.²⁵ In Fig. 7 we illustrate the fluid-flow paths for the four extremes of the Koch-curve geometries we have considered. The results of our calculations are summarized in Table II and Fig. 8. This model allows us to vary the channel cross-sectional size and the degree of surface

roughness independently. In Fig. 8 the different permeability estimates are compared for the first- and fourth-order Koch-curve models. In both cases we consider three values of the channel cross-sectional size. We see that the diffusion bound (7) greatly overestimates the permeability in every case. Here, as in the GC model, this estimate is based on an effective pore size but is relatively insensitive to the channel cross-sectional sizes that control the transport properties. The Kozeny-Carman estimate, which is controlled by variations in the surface area rather than the throat size, overestimates k in the smooth surface models but obviously can underestimate k as the surface roughness is increased. Only the estimate based on the Λ parameter, which responds directly to variations in the channel cross-sectional size, tracks quite closely to the exact permeability.

The Koch-curve model provides a rather severe test of permeability estimation. Indeed, we see that at a given

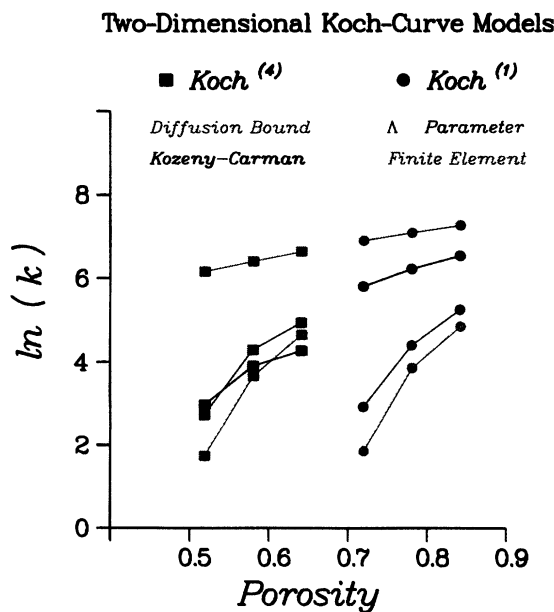


FIG. 8. For the first-generation (Koch⁽¹⁾) and fourth-generation (Koch⁽⁴⁾) two-dimensional Koch-curve models, exact calculations of the permeability are compared with the Kozeny-Carman and Λ parameter estimates, and with the diffusion bound of Eq. (7). The unit of length is chosen as in Table II.

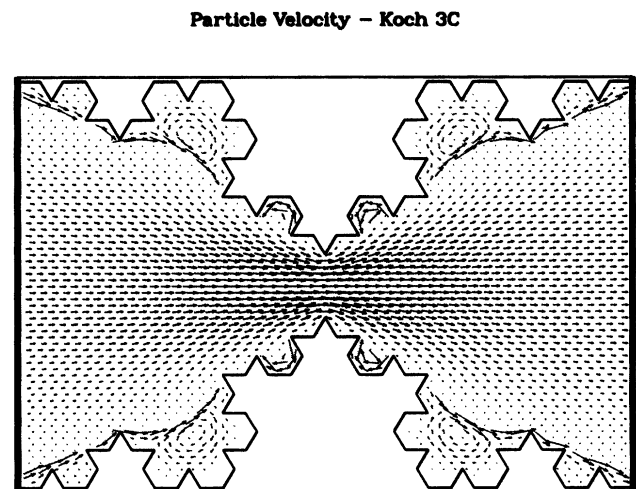


FIG. 9. Vortex flow is illustrated for the third-generation (Koch⁽³⁾) model. Here the cyan velocity vectors have had their magnitudes enhanced by a factor of 75 relative to those in the main flow path.

level of roughness, as the throat size is decreased the amount by which k_Λ overestimates k increases. The physics in this regime is controlled by the singularities associated with triangular tips that form the effective flow-channels. Because the fluid velocity must vanish at the interface, the influence of the electric-field singularities extends farther into the pore space than does the influence of those associated with the fluid-flow problem. When the channel cross-sectional areas are small enough that the singularities centered on the opposing tips overlap, we might reasonably expect to see significant differences between the electrical and fluid-flow problems. (Note that the situation here is quite different than that encountered in the GC model where, even as the system approaches its threshold, there are no singularities in the interface structure.) A further difference is associated with the fact that vortices can be set up in the fluid-flow problem that will dissipate energy and lead to lower permeabilities than might be estimated from the irrotational electric-field problem. This phenomena is illustrated in Fig. 9, where it is clear that the vortex flow is limited to regions of the pore space that are, in a sense, shielded from the main transport path. While this effect is not very significant in the Koch-curve model, in more complex geometries, where tortuosity and surface roughness are comingled, it may contribute significantly to the differences between electrical and fluid transport.

IV. CONCLUSIONS

We have employed a number of two- and three-dimensional models to study the relationship between different size parameters in porous media. In particular, we are interested in the length scale associated with the transport of viscous fluids. The results presented here show quite clearly that the Λ parameter, together with the electrical formation factor F , provides the most reliable permeability estimate. In summary, our most important results are the following.

(i) For the GC model, k_Λ yields an accurate estimate of k over the entire consolidated porosity range. In addition, k_Λ exhibits the proper analytic behavior as $\phi \rightarrow \phi_c$, the percolation threshold. In this limit, we have evaluated M_Λ exactly for sc, fcc, and bcc packings. In disordered versions of the GC model k_Λ again exhibits the proper analytic behavior as $\phi \rightarrow \phi_c$.

(ii) In the two-dimensional tortuosity models, where the pore space is characterized by a single length scale, one might expect there to be little difference between alternate permeability estimates. However, even here we find that k_Λ clearly provides the most accurate estimate.

(iii) In the Koch-curve models, where the pore geometry has features over a broad range of lengths, k_Λ is the only estimate that can track the variation of permeability as the porosity, effective flow-channel cross-sectional size, and surface roughness are varied.

(iv) Our results indicate those conditions under which k_Λ might be expected to depart significantly from the true permeability. Examples are (1) if transport is not dominated by pore \rightarrow throat \rightarrow pore sequences (as in the high-porosity limit of the GC model) and (2) if the structure of the pore throats leads to singularities in the flow and electric fields whose character controls the overall transport.

Note added in proof. In a recent article, M. Avellaneda and S. Torquato [Phys. Fluids A **9**, 2529 (1991)] have shown why our definition of Λ is not equivalent to the one given by Sheng and Zhou.¹⁸ In Appendix D of their paper a proper treatment of the Sheng and Zhou approach is shown to lead to our Eq. (4) rather than to Eq. (30) of Ref. 18.

ACKNOWLEDGMENTS

Part of this work was carried out while S. Kostek was on leave from Schlumberger-Doll Research, at the Department of Earth, Atmospheric, and Planetary Sciences, Massachusetts Institute of Technology, Cambridge, MA.

¹A. E. Scheidegger, *The Physics of Flow Through Porous Media*, 2nd ed. (University of Toronto Press, Toronto, 1974).
²J. Happel and H. Brenner, *Low Reynolds Number Hydrodynamics* (Martinus Nijhoff, The Hague, 1983).
³B. F. Swanson, J. Pet. Technol. **33**, 2498, 1981.
⁴A. J. Katz and A. H. Thompson, Phys. Rev. B **34**, 8179 (1986).
⁵W. E. Kenyon, P. I. Day, C. Straley, and J. F. Willemsen, SPE Form. Eval. **3**, 622 (1988).
⁶J. G. Berryman and S. C. Blair, J. Appl. Phys. **60**, 1930 (1986); J. G. Berryman, *ibid.* **57**, 2374 (1985).
⁷C. Straley, A. Matteson, S. Feng, L. M. Schwartz, W. E. Kenyon, and J. R. Banavar, Appl. Phys. Lett. **51**, 1146 (1987).
⁸A. Timur, J. Pet. Technol. **21**, 775 (1969); Log Anal. **10**(1), 3 (1969); (unpublished).
⁹D. L. Johnson, J. Koplik, and L. M. Schwartz, Phys. Rev. Lett. **57**, 2564 (1986).

¹⁰S. Torquato, Phys. Rev. Lett. **64**, 2644 (1990).

¹¹J. R. Banavar and D. L. Johnson, Phys. Rev. B **35**, 7283 (1987).

¹²H. J. Lugt and E. W. Schwiderski, Proc. R. Soc. London, Sect. A **285**, 382 (1965).

¹³E. R. Weibel, *Stereological Methods* (Academic, London, 1979), Vol. 2, Chap. 3.

¹⁴D. Wilkinson, D. L. Johnson, and L. M. Schwartz, Phys. Rev. B **44**, 4960 (1991).

¹⁵R. E. Larson and J. J. L. Higdon, Phys. Fluids A **1**, 38 (1989).

¹⁶R. Peyret and T. D. Taylor, *Computational Methods for Fluid Flow*, Springer Series in Computational Physics (Springer-Verlag, New York, 1983), Chap. 7.

¹⁷J. N. Roberts and L. M. Schwartz, Phys. Rev. B **31**, 5990 (1985); L. M. Schwartz and S. Kimminau, Geophysics **52**, 1402 (1987).

- ¹⁸P. Sheng and M.-Y. Zhou, *Phys. Rev. Lett.* **61**, 1591 (1988); M.-Y. Zhou and P. Sheng, *Phys. Rev. B* **39**, 12 027 (1989).
- ¹⁹B. I. Halperin, S. Feng, and P. N. Sen, *Phys. Rev. Lett.* **54**, 2391 (1985).
- ²⁰J. R. Banavar, M. Cieplak, and D. L. Johnson, *Phys. Rev. B* **37**, 7975 (1988).
- ²¹R. B. Saeger, L. E. Scriven, and H. T. Davis, *Phys. Rev. A* **44**, 5087 (1992).
- ²²D. H. Rothman, *Geophysics* **53**, 509 (1988).
- ²³S. Kostek, A. K. Gunstensen, and D. H. Rothman (unpublished).
- ²⁴*Physics and Chemistry of Porous Media— II (Schlumberger-Doll Research, Ridgefield, CT, 1986)*, Proceedings of the Second International Symposium on the Physics and Chemistry of Porous Media, edited by J. R. Banavar, J. Koplik, and K. W. Winkler, AIP Conf. Proc. No. 154 (AIP, New York, 1987).
- ²⁵P. Wong, J. Howard, and J. Lin, *Phys. Rev. Lett.* **57**, 637 (1986).
- ²⁶L. M. Schwartz, P. N. Sen, and D. L. Johnson, *Phys. Rev. B* **40**, 2450 (1989).

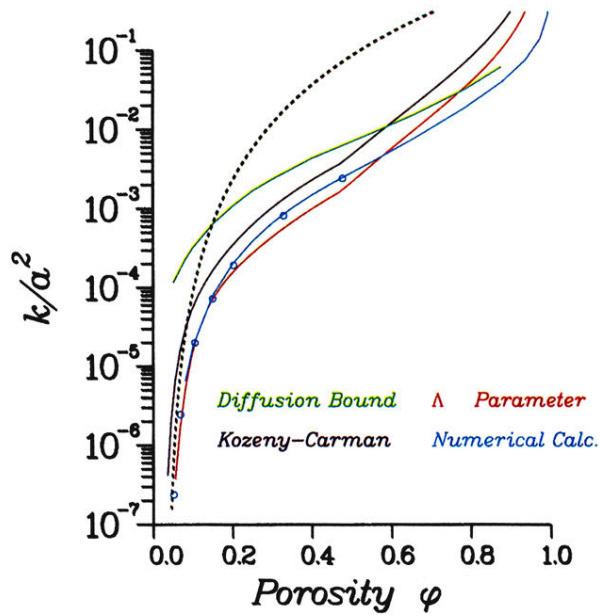


FIG. 3. For the simple cubic GC model, exact calculations of the permeability (solid cyan line, Ref. 15; open cyan circles, Ref. 18) are compared with the Kozeny-Carman and Λ -parameter estimates, with the diffusion bound (Ref. 10), and with the asymptotic formula (19) (dashed line). The values of Λ used here are the ones shown in the solid curve of Fig. 2. Here the length units are as in Fig. 2.

Tortuosity Models

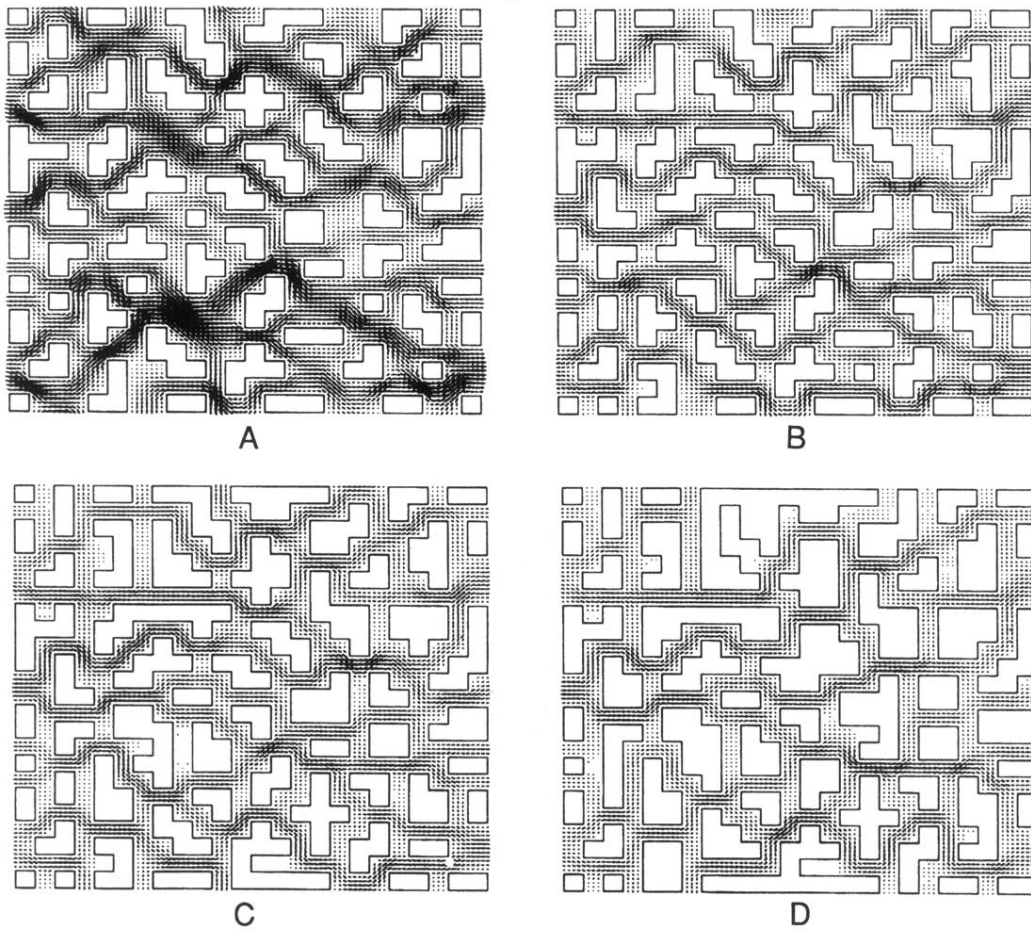


FIG. 5. The four two-dimensional tortuous-path models are pictured with the fluid-flow vectors shown in their pore spaces.

Two-Dimensional Tortuosity Models

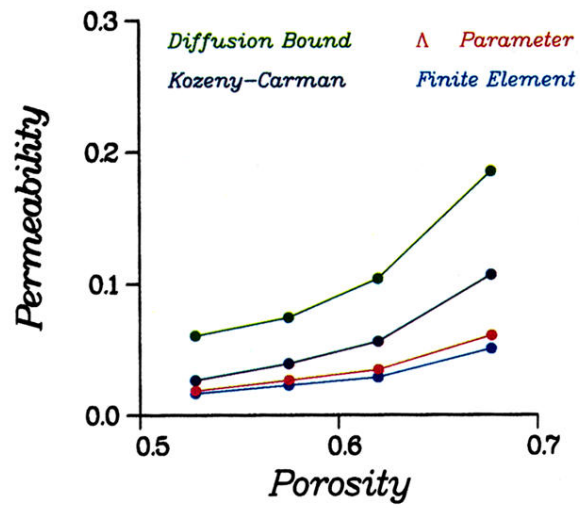


FIG. 6. For the tortuous-path models, exact calculations of the permeability are compared with the Kozeny-Carman and Λ -parameter estimates, and with the diffusion bound of Eq. (7). The unit of length is chosen as in Table I.

Two-Dimensional Koch-Curve Models

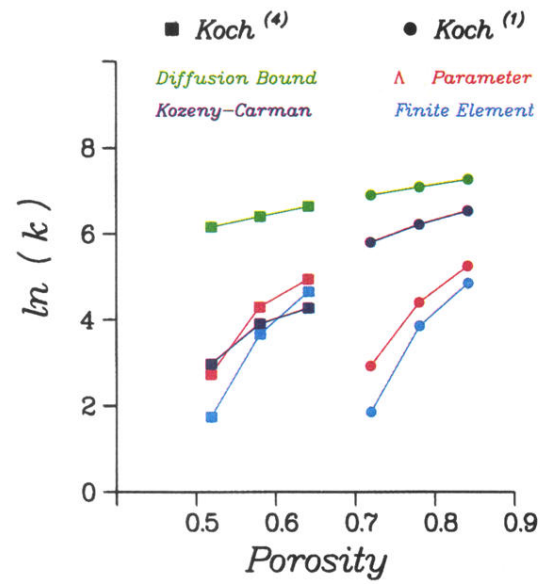


FIG. 8. For the first-generation (Koch⁽¹⁾) and fourth-generation (Koch⁽⁴⁾) two-dimensional Koch-curve models, exact calculations of the permeability are compared with the Kozeny-Carman and Λ parameter estimates, and with the diffusion bound of Eq. (7). The unit of length is chosen as in Table II.

Particle Velocity – Koch 3C

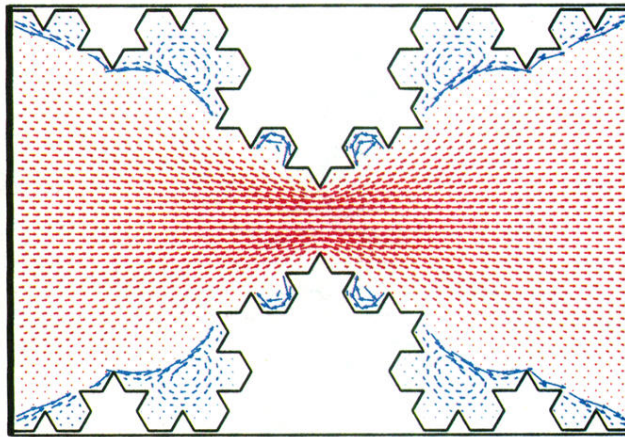


FIG. 9. Vortex flow is illustrated for the third-generation (Koch⁽³⁾) model. Here the cyan velocity vectors have had their magnitudes enhanced by a factor of 75 relative to those in the main flow path.